Received: 17 January 2025 | Revised: 24 May 2025 | Accepted: 24 May 2025

DOI: 10.1002/dvdy.70059

RESEARCH ARTICLE

Developmental Dynamics | AMERICAN ASSOCIATION FOR ANATOMY | WILEY

Identification of neural crest and melanoma cancer cell invasion and migration genes using high-throughput screening and deep attention networks

J. C. Kasemeier-Kulesa[1] | **S. Martina Perez**[2] | **R. E. Baker**[2] | **P. M. Kulesa**[3]

[1]Stowers Institute for Medical Research, Kansas City, Missouri, USA

[2]Wolfson Centre for Mathematical Biology, Mathematical Institute, University of Oxford, Oxford, UK

[3]Children's Mercy Research Institute, Children's Mercy Hospital, Kansas City, Missouri, USA

Correspondence
S. Martina Perez, Wolfson Centre for Mathematical Biology, Mathematical Institute, University of Oxford, Woodstock Road, Oxford, OX2 6GG, UK.
Email: simon.martina-perez@magd.ox.ac.uk

Funding information
Eunice Kennedy Shriver National Institute of Child Health and Human Development, Grant/Award Number: R03-HD105079-02

Abstract

Background: Cell migration and invasion are well-coordinated in development and disease but remain poorly understood. We previously showed that the neural crest (NC) cell migratory wavefront shares a 45-gene panel with other cell invasion phenomena. To rapidly and systematically identify critical genes, we performed a high-throughput siRNA screen and statistical and deep learning analyses to determine changes in NC- versus non-NC-derived human cell line behaviors.

Results: We find 14 out of 45 genes significantly reduced c8161 melanoma cell migration; four of the 14 genes altered leader cell motility (BMP4, ITGB1, KCNE3, and RASGRP1). Deep learning identified marked disruptions in cell-neighbor interactions after BMP4 or RASGRP1 knockdown in c8161 cells. Recombinant proteins added to the culture media revealed five out of the 11 known secreted molecules stimulated c8161 cell migration. BMP4 knockdown severely reduced c8161 in vivo invasion in a chick embryo transplant model. Addition of BMP4 protein to the culture media of BMP4-siRNA-treated c8161 cells rescued cell migratory ability.

J. C. Kasemeier-Kulesa and S. Martina Perez are shared co-first authorship.

In Memoriam: Paul Kulesa: Paul gained his doctorate in mathematical biology under the supervision of Professor J.D. Murray. As a theoretician, Paul felt frustrated that model predictions were rarely tested, so he trained as an experimentalist under the guidance of Professor Scott Fraser. This gave him the powerful set of combined skills in being able to determine which biological questions were amenable to mathematical modeling and which were not. Thus began a fruitful collaboration between us and the Kulesa laboratory that spanned over a decade. During this time, we combined theory with experiment to unearth a number of key findings in NC biology. Paul was an excellent scientist, always full of new ideas and very passionate about combining mathematics with biology to lead to insights that could not be achieved by either discipline alone. He was also very warm, kind, and supportive, with a cheeky sense of humor that always made us laugh. He leaves behind his wife, Jennifer Kasemeier-Kulesa, who is also a Senior Researcher in his lab, and five children. Paul will be sorely missed by all who knew him, but he leaves behind a rich legacy of scientific work that will live long into the future.

Conclusion: High-throughput screening and deep learning distilled a 45-gene panel to a small subset of genes critical to melanoma and warrant deeper in vivo functional analysis for their role and potential synergies in driving NC cell migration and invasion.

KEYWORDS

attention networks, cell invasion, deep learning, high-throughput, melanoma, migration, neural crest, siRNA screen

1 | INTRODUCTION

Cell migration and invasion are well-coordinated processes in early development, cancer, the immune response, and wound healing that, if uncontrolled, can lead to severe birth defects and life-threatening disease. The neural crest (NC) serves as a model for cell invasion and collective migration during vertebrate development[1–3] and for several invasive human mesenchymal cancers, including NC-derived melanoma.[4–6] NC cells are essential to vertebrate embryogenesis, traveling long distances after exiting the dorsal neural tube to contribute to nearly every peripheral organ.[7] Although NC cells emerge all along the anteroposterior axis and are sculpted into discrete streams that invade immature extracellular matrix (ECM) and loose mesoderm, the molecular mechanisms that underlie invasion and collective cell migration remain unclear. Mistakes in NC cell migration led to birth defects, termed neurocristopathies, that include shortened lower jaw and cleft lip and palate in the head, and failure to reach the end of the embryonic gut or Hirschsprung's disease.[8,9] Therefore, by leveraging the accessibility of the NC to advances in spatial gene profiling and their ancestral relationship to melanoma, identification and functional analysis of a critical set of cell invasion genes have the potential to inform strategies to repair human neurocristopathies and control cancer metastasis.

Single cell transcriptome analyses have made clear that there is tremendous spatial molecular heterogeneity within a discrete NC cell migratory stream.[10–12] In the chick head, isolation and profiling of cranial NC cells at distinct, progressive time points during migration within the second branchial arch (BA2) stream revealed that leader NC cells have a novel transcriptional signature that is consistent and enriched for approximately 900 genes.[10] Subsequent study of the cellular landscape of the first four chick cranial to cardiac branchial arches (BA1-4) using label-free, unsorted single-cell RNA sequencing identified 266 invasion genes out of the original list (>900 genes[10]) common to all four BA1-4 NC cell migratory streams.[11] In support of transcriptional differences within NC cell migratory streams throughout the embryo, single cell RNA-seq analysis of isolated leader and follower enteric neural crest-derived cells (ENCDCs) showed that leader ENCDCs are transcriptionally distinct from followers, exhibiting altered expression of ECM and cytoskeletal genes consistent with an invasive phenotype.[13] Wavefront-ENCDCs also lacked expression of genes related to neuronal or glial maturation, present in follower cells[13] and support recent results showing zebrafish NC cell lineage decisions are made during mid-migration rather than at the end target.[12] Although these transcriptional data offer an opportunity to better understand NC cell invasion and collective cell migration mechanisms, the future studies typically to determine the function of individual genes derived from large-scale transcriptional analyses are time-prohibitive and impractical.

To address this challenge, high-throughput screening offers a rapid means to analyze large transcriptional data with an initial prioritization relevant to cell migration and invasion. Unfortunately, dissection and isolation of large numbers of embryonic NC cells in any current model organism with the purpose to seed multiple, multi-well high-throughput assays are extremely labor-intensive and unreasonable. To overcome this, the readily available NC-derived human metastatic melanoma c8161 cell line, which displays similar behaviors to embryonic NC cells[6,14,15] including aggressive invasion and collective cell migration, can instead be used. Knockdown of individual genes using siRNA transfection (Table 1) in cell culture offers a straightforward means to molecularly perturb gene function and, when combined with a high-throughput assay and time-lapse confocal microscopy, permits quantification and comparison of changes in cell migratory behaviors and invasion.

Collective cell migration and invasion are critical in a wide range of diverse biological phenomena, including embryogenesis, wound repair, the immune response, and cancer metastasis. Since the NC is widely utilized as a model system to study collective cell migration and invasion mechanisms, a list of 34 published gene signatures was curated from other invasive cell types and compared to the embryonic NC cell invasion signature.[11] This comparison revealed a subset of 45 out of greater than 900 genes of the chick leader cranial NC cell invasion

TABLE 1 SiRNAs used on 45-gene panel list.

C8161 + HT1080 inhibitors	C8161 Specific Inhibitor	HT1080 Specific Inhibitors	C8161 Agonists
ARPC3	BMP4	CA2	KITLG
PRKCQ	IFI30	DPYD	RASGRP3
RASGRP3	IL13RA1	HSPB1	VEGFC
CREB3L2	INHBA	INHBA	
ITGB1	JUN	MMP11	
UNC5B	KYNU		
	NEXN		
	NRP1		
	RAC2		
	RASGRP1		
	SERPINI1		
	SH3TC1		
	TUBB6		
	UPP1		
	VIM		

signature in common with two or more cell invasion signatures from this list.[11] This condensed signature of 45 genes, although not encapsulating all genes necessary for cell migratory and invasive characteristics, is manageable for a high-throughput siRNA screening assay to prioritize a smaller subset of genes for single gene in vivo functional studies of NC cell migration. Results of such a screening assay will also help to determine whether these 45 genes have a conserved function in non-NC-derived cell types and, more broadly, to other cell migration and invasion phenomena.

In this study, we compared changes in cell dynamics in human metastatic melanoma c8161 versus human fibrosarcoma HT1080 cell lines after siRNA gene knockdown. We employed these two human cell lines since they together allow lineage-specific and technical comparisons. First, C8161 metastatic melanoma cells are neural-crest-derived and display leader–follower collective migration and long-range invasion highly reminiscent of cranial NC streams,[14,15] and are thus a malignant analogue of the embryonic NC cells that generated our 45-gene panel. The c8161 cell line is also readily transfected, robust in the plugged-stopper assay, and has been validated in our chick-embryo transplant model, permitting seamless in-vitro/in-vivo correlation. HT1080 fibrosarcoma cells provide a mesoderm-derived, highly motile but non-neural-crest control. They close free space at a rate comparable to c8161 melanoma cells under identical culture conditions, lack the NC invasion signature, and are equally amenable to siRNA transfection and live imaging. Taken together, this pair of lines allows us to distinguish invasion mechanisms specific to NC-derived malignancy from general perturbations of collective mesenchymal migration.

Using a plugged plate assay in which cells are seeded around a rubber stopper, open space closure rates, as well as the dynamics of edge (leader) and bulk (follower) cells, were measured after siRNA gene knockdown and rubber stopper removal, as well as the dynamics of edge (leader) and bulk (follower) cells into open free space to determine significant changes in cell invasion and collective cell migration. We then used deep learning attention network analysis of large-scale cell trajectory data generated from each of the gene knockdowns to identify alterations in cell neighbor interactions. Separately, we performed an analysis of the known secreted molecules of the 45-gene panel by comparing changes in c8161 cell migration after the addition of the recombinant proteins in the culture media. Together, these experiments identify a subset of the 45 gene invasion signature that affects melanoma cell migration and warrants further in-depth analysis.

2 | RESULTS

2.1 | A rubber stopper high-throughput screening assay avoided physical damage of cell membranes and provided a uniform intact circular migratory wavefront for analysis of open free space invasion and collective cell migration

To systematically test our novel 45-gene invasion signature derived from a comparison between the embryonic cranial NC cells and a broad range of other cell invasion phenomena (Figure 1A), we used a high-throughput rubber stopper-based screening assay to study human c8161 melanoma versus HT1080 fibrosarcoma cell lines (Figure 1B). Each cell line was transfected with siRNAs to knock down single genes in duplicate from the 45-gene panel prior to seeding cells in rubber stopper-plugged plates (along with water and negative siRNAs for controls). After seeding and adherence of cells in each well, the plugs were removed from each well and cell trajectories were collected from 24 hr. time-lapse confocal imaging sessions (Figure 1B, C). Open free space was defined as the area created by removal of the rubber stopper plug in each well. In addition, removal of the rubber stopper did not disrupt cell integrity and provided a uniform circular wavefront (Figure 1C), in contrast to the typical wound closure associated with scratch assays. Cell dynamics data was analyzed using traditional

metrics (for example, mean-square displacement and directionality) as well as using deep learning networks to study changes in cell-neighbor relationships after siRNA knockdown of each of our 45-gene panel (Figure 1D). Lastly, we analyzed the 45-gene panel for upstream transcription factors (Figure 1E).

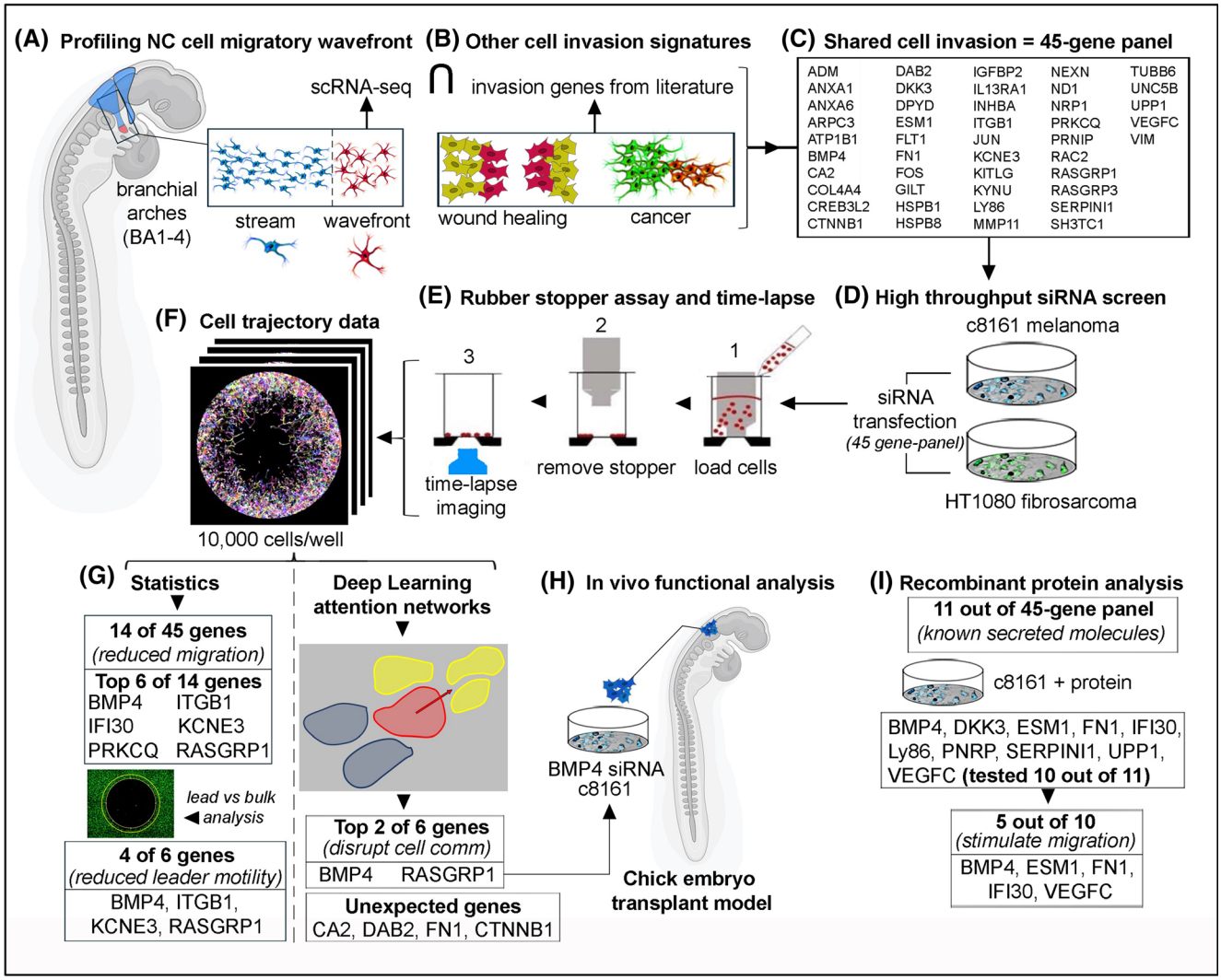

FIGURE 1 Schematic of integrated experimental and computational workflow of high throughput screening assay and cell behavior analytics. (A) Cranial neural crest (NC) cell migration in the vertebrate head in discrete streams with a migratory wavefront (red) and follower NC cells (blue). (A), (B) Comparison of genes enhanced within chick NC cells at the migratory wavefront (acquired by single cell RNA seq) and published invasion signatures from a wide range of other cell invasion phenomena. The upsidedown U indicates intersection of the gene lists in which the NC gene was included in at least two of the published invasion signature lists, resulting in a (C) 45-gene panel. (D) High-throughput screen compares changes in cell migration and invasion behaviors of human c8161 metastatic melanoma versus HT1080 human fibrosarcoma cells after gene knockdown using siRNA. (E) A plugged plate assay allows for loading of transfected cells, removal of the rubber stopper and subsequent confocal time-lapse imaging to (F) generate dynamic cell trajectory data, typically greater than 10,000 cells per well. (G, left-hand side) Statistical analyses of the fluorescently labeled cell trajectories for all gene knockdowns identified critical genes listed (top 6 of 14 out of 45), including analysis of the leaders within the migratory wavefront of the circle (shown in the inset) versus followers to show reduced leader motility (4 out of the top 6 genes). (G, right-hand side) Deep learning network analysis analyzed changes in cell-neighbor interactions and identified two genes (BMP4 and RASGRP1) and validated genes previously implicated in other cell migration phenomena but did not show changes in melanoma migration and invasion, which we termed unexpected genes ($n = 4$) that altered cell-neighbor interactions after knockdown. (H) Our chick embryo transplant model served as an in vivo assay to ascertain changes in cell migration and invasion after gene knockdown, which we show as BMP4-siRNA c8161 cells. (I) Recombinant protein analysis performed separately and static analysis to determine changes in open space closure in the presence of 11 out of 45-gene panel known secreted molecules ($n = 10$ out of 11 molecules tested) added to the culture media and using the same plugged plate assay.

2.2 | The invasion of c8161 melanoma cells into open free space is significantly affected by the knockdown of 14 out of 45 genes that primarily affect cell motility rather than proliferation

To identify siRNA knockdowns linked to dynamic changes in human cancer cell behavior during free space closure, we first conducted a statistical analysis of changes in free space area and cell count (Figure 2). For each well, we computed *z*-statistics for the free space area and cell count fold change. We present gene knockdowns that significantly affected free space closure defects and find 14 out of 45 genes (BMP4, FN1, FOS, IFI30, IL13RA1, ITGB1, KCNE3, KYNU, NEXN, PRKCQ, RASGRP1, SH3TC1, UPP1, and VIM) included in the screen resulted in significant free space closure in the c8161 melanoma cells (Figure 2A). BMP4, ITGB1, IFI30, KCNE3, PRKCQ, and RASGRP1 ranked in the top six out of 14 (Figure 2A). Strikingly, in the HT1080 fibrosarcoma cells, only four out of 14 genes exhibited significantly reduced free space closure (BMP4, ITGB1, KCNE3, and RASGRP1; highlighted in orange and shared with the top six genes of the c8161 melanoma cells in Figure 2A).

To better understand the interplay between cell proliferation and cell motility during free space closure, we compared the two characteristics. In the c8161 melanoma cells, only BMP4 knockdown inhibited free space closure in conjunction with significantly reduced cell proliferation (Figure 2A; first row, shaded in red). Other knockdowns of 14 out of 45 genes that exhibited a reduced rate of free space closure (e.g., ITGB1, KCNE3, and RASGRP1) did not show significantly altered cell proliferation in the c8161 melanoma cells (Figure 2A). FN1 and FOS knockdowns in the c8161 melanoma cells showed significantly improved free space closure rates, and both gene knockdowns also exhibited significantly reduced cell proliferation (Figure 2A; rows 2–3 and columns 1–2). Likewise, no gene knockdowns in the c8161 melanoma cell line data set were associated with a reduced rate of free space closure and enhanced cell proliferation or both an enhanced rate of free space closure and increased cell proliferation (Figure 2A). In contrast, cell proliferation and cell motility in the HT1080 fibrosarcoma cells were impacted, with a reduction of cell proliferation the more pronounced effect. Together, these data suggest that in c8161 melanoma cells the set of gene knockdowns primarily affected free space closure through changes in cell motility, rather than through cell proliferation. The gene knockdowns influenced both cell motility and cell proliferation in the HT1080 fibrosarcoma cells but were more strongly associated with reduced cell proliferation.

2.3 | c8161 melanoma cells exhibit collective cell migration with a leading edge subpopulation that rapidly migrates in a directed manner to fill up open free space, regardless of gene knockdown

The preceding statistical analysis of open free space areas and cell count fold changes suggested that invasion is driven by cell motility in the c8161 melanoma cells but did not precisely identify which changes in motility at the cell level contributed to reduced or enhanced free space closure. To address this, we performed cell tracking to investigate the motility properties of individual cells more thoroughly.

NC cells are well-known for their leader-follower dynamics, whereby leader cells must invade through immature ECM, loosely connected mesoderm, and other cell types to pave the way for follower cells to move collectively behind the wavefront.[11] To better understand whether the gene knockdowns in the screen perturb this pattern, we tracked c8161 melanoma and HT1080 fibrosarcoma cell trajectories throughout the free space closure process (Figure 2B–H). In each of the wells, we tracked all cells in the field of view and computed the average displacement per frame for each cell. By making a distinction between cells at the leading (edge) versus cells in the follower (bulk) subpopulation, we computed the displacement difference between edge and bulk cells for each of the different wells, defined as the difference between the mean edge and the mean bulk cell displacement.

The displacement difference acts as a measure for how motile on average the cells at the edge of the collective are relative to those in the bulk subpopulation. A large displacement difference would indicate a highly active edge subpopulation that rapidly invades toward the center of the free space, with a less actively motile bulk population. Similarly, we computed the average directionality in the direction of the free space for each cell and determined the directionality difference as the difference between the average directionality for cells at the edge and that for cells in the bulk (Figure 2B, inset). We find that c8161 melanoma cell edge subpopulations display significant differences in motility and directionality compared to the HT1080 fibrosarcoma cells across the different gene knockdowns (Figure 2C, D). This finding suggests that c8161 melanoma but not non-NC-derived HT1080 cells exhibit an edge subpopulation that rapidly migrates in a directed manner to fill up free space, regardless of gene knockdown.

We next compared the displacement difference directly to free space closure (Figure 2E, F). We find that for the c8161 melanoma cells, an edge subpopulation with enhanced motility leads to enhanced free space

(A)

Gene KD	c8161 Area change	c8161 Cell change	HT1080 Area change	HT1080 Cell change
BMP4	5.76	1.03	2.28	2.24
FN1	1.09	1.24	1.08	2.36
FOS	1.14	1.22	0.80	2.34
IFI30	4.34	1.36	1.64	2.19
IL13RA1	3.59	1.35	1.68	2.25
ITGB1	4.55	1.35	2.38	2.09
KCNE3	4.13	1.36	2.38	2.22
KYNU	3.91	1.33	1.77	2.21
NEXN	3.80	1.37	1.79	2.24
Neg	2.45	1.39	1.19	2.31
PRKCQ	4.09	1.35	1.33	2.09
RASGRP1	4.00	1.37	3.30	2.11
SH3TC1	3.71	1.34	1.86	2.16
UPP1	3.44	1.33	1.24	2.12
VIM	3.82	1.36	1.51	2.23

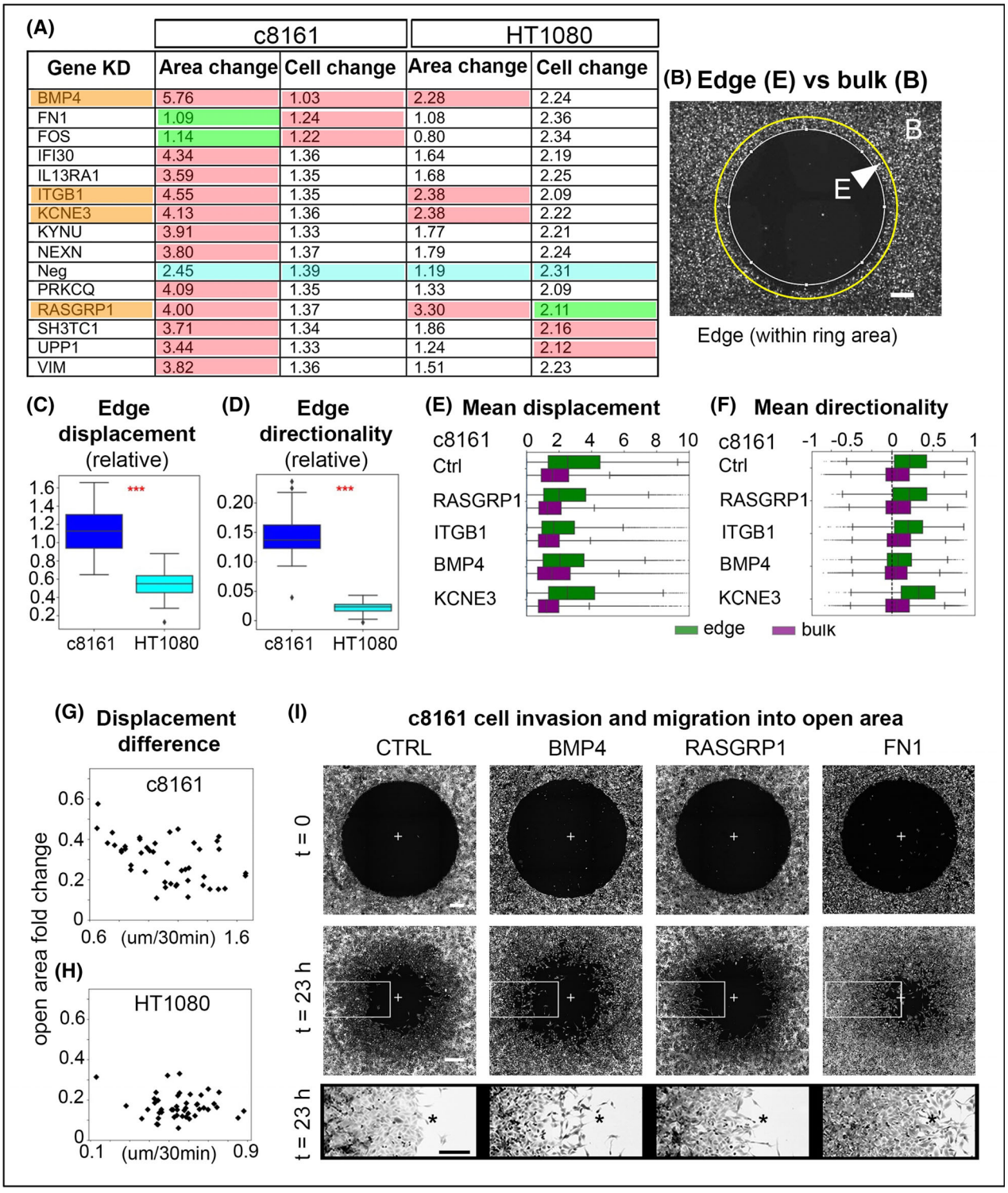

FIGURE 2 Quantitative metrics of open area closure and migration. (A) Table of genes resulting in significantly reduced wound closure in the c8161 cell line with fold changes for wound area and cell count fold changes (B) TrackMate tracks overlayed for cells in the edge region (C) relative edge displacement across all experiments using c8161 and HT1080 cells. (D) Relative edge directionalities across all experiments using c8161 and HT1080 cells. (E) Mean displacement in edge and bulk regions in the c8161 cell line. (F) Mean directionality in edge and bulk regions in the c8161 cell line. (G) Displacement difference versus wound closure for all considered c8161 biological replicates. (H) Directionality difference versus wound closure for all considered HT1080 biological replicates. (I) Typical images collected from time-lapse imaging sessions of high throughput screen at start (0 h) and near the end (23 h) of 24 h time-lapse sessions for Control siRNA (CTRL), BMP4, RASGRP1, and FN1 siRNA knockdowns. In the bottom row of images, the leading edge is migrating from left to right (center of well is marked by plus sign and leading edge with an asterisk). The scalebars are all 100 μm.

closure (Figure 2G; Spearman correlation coefficient of −0.452, p-value = .00180); a trend not observed in HT1080 fibrosarcoma cells (Figure 2H). Together, this suggests that for c8161 melanoma cells the active leader cells within the edge subpopulation are most successful in closing the free space, in contrast to when all cells in the collective migrate according to the same rules. Lastly, the same analysis for the directionality difference showed no direct relationship with closure of the free space for the HT1080 fibrosarcoma cells.

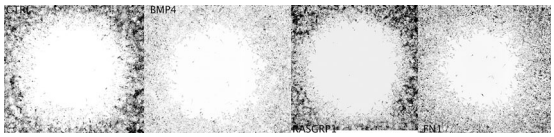

MOVIE 1 Time-lapse imaging sequence of human c8161 metastatic melanoma cell behaviors in response to knockdown of Bmp4, Rasgrp1, Fn1, and Control. There are 45 images taken from the sequence of images collected every 30 min for 24 h. Playback speed is 10 frames/s.
Video content can be viewed at https://onlinelibrary.wiley.com/doi/10.1002/dvdy.70059

2.4 | Leader cell motility is impaired after knockdown of BMP4, ITGB1, KCNE3, or RASGRP1, with only BMP4 knockdown also exhibiting less-directed, more wandering c8161 melanoma cell behaviors

Since our cell trajectory analysis suggested that highly motile leader cells are associated with faster free space closure (Figure 2E; c8161 melanoma cells), we examined whether the set of gene knockdowns that result in reduced free space closure also exhibited a reduction in relative edge displacements. Indeed, leader c8161 melanoma cell motility is reduced by as much as 30% in the BMP4, ITGB1, KCNE3, and RASGRP1 knockdowns, with a mean cell speed of 5.1, 4.4, 4.5, and 5.2 μm/h, respectively, compared to 6.4 um/h in controls (Figure 2G). Furthermore, by characterizing the difference between displacement for leader versus bulk cells, we find that BMP4, ITGB1, and RASGRP1 knockdowns also exhibit a marked, reduced difference between leader and bulk cell motility. This was evident by the overlap in the interquartile range, contrary to the trend in control and KCNE3 (Figure 2E). Interestingly, only BMP4 exhibited a reduction of leader cell directionality (0.094 vs. 0.23 for control (Figure 2H)), establishing that loss of BMP4 gives rise to less-directed, more wandering c8161 melanoma cell behaviors at the leading edge (Figure 2I; see Movie 1). Differences in the free space closure and spacing between the leader and follower cells are markedly noticeable in the static images extracted from typical time-lapse imaging, showing Control versus BMP4, RASGRP1, and FN1 knockdowns (Figure 2I; see Movie 1).

Performing this analysis on the remaining 10 out of the 14 gene knockdowns in c8161 melanoma cells that result in reduced free space closure (Figure 2A; not significant in HT1080 fibrosarcoma cells), we find that all 10 genes except PRNP have significantly reduced edge cell displacement. No gene knockdown showed altered edge directionality as compared to the controls. These findings suggest that the cluster of gene knockdowns exhibited reduced free space closure due to inhibited leader cell motility. Furthermore, BMP4, ITGB1, and RASGRP1 also show a loss of leader cell-type behavior by displaying a larger difference between leader and follower cell motility. Finally, we remark that both FN1 and FOS knockdowns (which have significantly higher rates of free space closure than control) show the same trend, exhibiting significantly more motile edge cells (see Movie 1 for FN1).

2.5 | Deep attention network analysis identified distinct cell–cell interaction patterns in collective cell migration of c8161 versus HT1080 cells and alterations after gene knockdown

We observed above that individual cell behaviors at the leading edge have an important impact on the rate of free space closure, but cells do not migrate in isolation; closure is an inherently cooperative process. Therefore, we asked whether any of the 45 genes in the high-throughput screen play a role in cell–cell communication during the closure process. However, as cell–cell communication cannot be directly observed from an in vitro assay, the patterns of cell–cell communication must be inferred from the large-scale cell trajectory data obtained by tracking individual cells in these assays. For the inference of cell–cell communication between collectively migrating agents (including, but not limited to, cells in a multicellular system such as a high-throughput assay), several frameworks exist. In this context, we are particularly interested in how cells communicate with their neighbors as a function of their relative spatial location. For example, cells close to the edge of the invading population are impacted by free space area they migrate into, which defines a clear 'front' polarity. Consequently, the migratory cue resulting from this guidance of collective migratory pressure into free space competes with the cues arising from interactions with neighboring cells. There currently exist various ways to quantify

interactions between neighboring migrating agents, with approaches generally focused around using short-term directional correlations to identify which neighbors have motion that is most correlated.[16,17] Such approaches are used in various contexts, for example swarming fish[17] or echolocating bats.[16] While all these frameworks provide valuable insights that could be extended to the context of collectively migrating cells, they have the shortcoming that correlations between agents do not isolate the role of relative position of the cells in pairwise interactions between cells, as other factors, such as distances, velocities, accelerations, and other neighbors, all influence such correlations. For this reason, we propose to use a framework that can explicitly quantify the influence of relative cell position on the pairwise interactions between neighboring cells.

Deep attention networks are a mathematical framework that enables quantitative measurement of the cell–cell interactions that most influence velocity alignment in a cellular collective. In brief, the deep attention network framework aims to estimate the probability that a given cell will move in a given direction, given the movements of the cells closest to it. The deep attention framework aims to do so by estimating two functions. The first function quantifies the importance of a cell's neighbors as a function of their location relative to the cell's direction of motion. The other function quantifies the impact of their velocities, accelerations, and distances to the resulting motion. These two functions are then approximated by two deep neural networks, which are trained using a large-scale data set of trajectories obtained from the high-throughput assay. The benefit of using a deep learning framework is that it provides a method to quantify probabilities associated with movement, which can be tested and validated, whereas measures of correlation between the motions of migrating agents do not make suggestions about the strength or the causality of the interactions. For more details, please see the methods section on deep attention networks.

We trained the attention networks on each of the different siRNA gene knockdown data sets to quantify cell–cell attention patterns. These analyses show that cells "pay attention" to a subset of neighbors such that only cells within a given region relative to the polarity axis of the cell influences the future direction of the cell (Figure 3A). In every attention map, the color bar is normalized from 0 (dark blue) to 1 (bright yellow). Bright-yellow sectors therefore pinpoint neighbor positions that the network predicts exert the strongest influence on the focal cell's next turn, whereas blue sectors indicate minimal influence. The fact that this high-attention region appears on just one side of the circle in many conditions reveals a previously unrecognized directional polarity in neighbor sensing. This observation underpins several of our key mechanistic conclusions.

We first established typical characteristic patterns of "attention" for c8161 melanoma and HT1080 fibrosarcoma cells in the absence of gene knockdown (Figure 3B, C). In this view, c8161 melanoma cells are characterized by a highly localized attention pattern at the front of the cell. In stark contrast, we find a very narrow front- and-back pattern of attention for the HT1080 fibrosarcoma cells (Figure 3C). This pattern is consistent with the typical sliding of cells in between each other in a largely non-coordinated fashion. Having characterized the baseline cell–cell attention patterns, we next turned to the question of whether the knockdown of any of the 45 genes would reveal attention patterns distinct from the wildtype scenario.

To better compare patterns of cell neighbor relationships between the different gene knockdowns, we extracted quantitative metrics that describe the patterns of attention. We quantified both the extent to which cells pay attention to neighbors in front and behind as well as the width of the attention field. The c8161 melanoma cells have a much wider attention pattern than HT1080 fibrosarcoma cells (Figure 3B, C). In addition, c8161 melanoma cells displayed a wide range of attention behaviors depending on gene knockdown (Figure 3D, E). Both the width of the cell–cell attention field as well as the front-to-back cell neighbor interactions were affected (Figure 3D). For example, we observed a wider attention range in the DAB2 knockdown that stretched from the front to along the sides of the cell, suggesting the cell–cell interactions were broadened to side-by-side neighbors (Figure 3D). In contrast, the knockdown of CA2 produced a pattern where regions ahead and behind the cell were largely ignored (Figure 3D). FN1 knockdown produced a pattern in the c8161 melanoma cells that resembled the wildtype HT1080 cells with a front-to-back pattern (compare Figure 3C with Figure 3D, F); FOS knockdown resembled the c8161 WT control pattern (compare Figure 3C with Figure 3F). In the CTNNB1 knockdown, cells appeared to pay attention to neighbors along the sides and behind rather than search for open free space (compare Figure 3B, D). Strikingly, in the HT1080 fibrosarcoma cells we find that there is no qualitative variation in attention patterns (data not shown), consistent with the observation that migration is highly collective in c8161 melanoma cell populations, but not in the HT1080 fibrosarcoma cell populations.

We next asked whether altered patterns of attention are associated with the observed free space closure changes. We compared the attention patterns for the four gene knockdowns leading to inhibited free space closure (BMP4, ITGB1, KCN3, and RASGRP1) with the attention

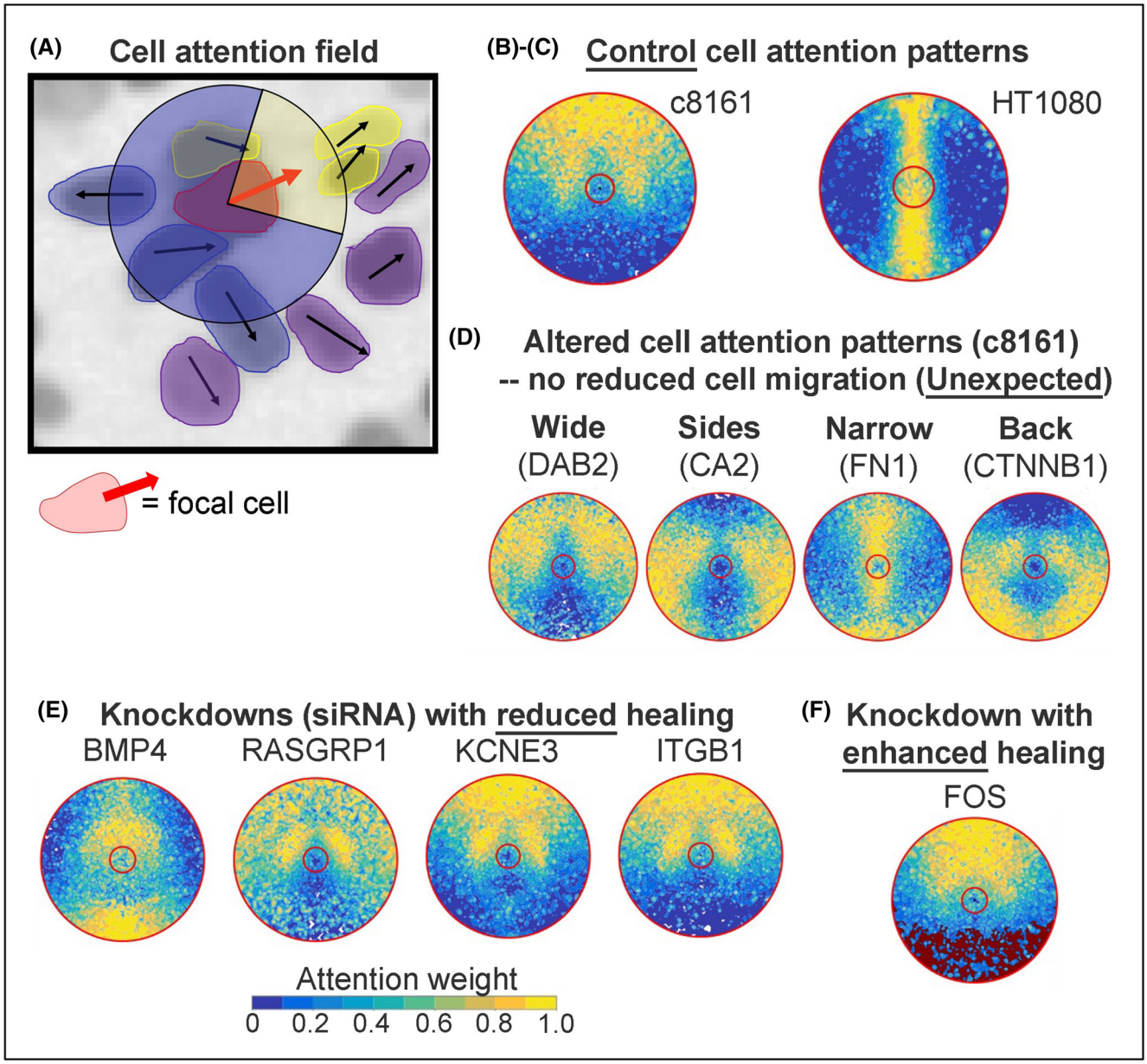

FIGURE 3 Deep learning network analysis reveals altered patterns of attention between migrating c8161 and HT1080 cells. (A) Schematic showing focal cell (red) with a cartoon attention cone. Cells in yellow are cells in the high attention region, cells in blue in the low attention region and cells in green are outside the attention range. (B), (C) Attention patterns for Neg knockdown controls in (B) in c8161 and (C) in HT1080 cells. (D) Effects of siRNA knockdown on attention network patterns, notably the width of the attention cone as well as the location to the front or back of the cell has a wide variability, and were unexpected for these genes that did not show reduced migration of cells in the plugged plate assay. (E) Attention networks for four siRNA knockdown perturbations that significantly affected wound closure rates (see Figure 2; BMP4 and RASGRP1 show altered cell attention patterns) and for (F) two siRNA knockdowns (FN1 shown in (D) and FOS shown in (F)) with enhanced healing. Throughout, warm colors denote higher inferred neighbor influence (bright yellow ≈1.0, the maximum of the normalized scale; dark blue ≈0). Asymmetry in the map—that is, a bright sector confined to one side of the circle—therefore reports polarity in neighbor sensing, a key biological result of this study. The two concentric red rings reproduce the inner ($r = 15$ μm) and outer ($R = 90$ μm) radial limits that we imposed when computing attention; only neighbors whose centers lie between r and R are supplied to the network.

patterns for the knockdowns that resulted in improved free space closure (Figure 3E). While loss of ITGB1 and KCNE3 retained the wildtype pattern of attention, both BMP4 and RASGRP1 knockdowns displayed altered attention patterns (Figure 3E). Importantly, these respective attention patterns were qualitatively different; loss of BMP4 displayed attention toward the front and back and loss of RASGRP1 showed attention only toward the front

(Figure 3E). Likewise, loss of FN1 and FOS promoted free space closure but showed no common qualitative features in the attention pattern (Figure 3F).

2.6 | Addition of recombinant proteins for five secreted genes of the 45-gene panel increases migration of c8161 melanoma cells in culture

Eleven of the genes from the 45-gene panel are known secreted molecules. To test whether the presence of any of these factors stimulates cell migration, we added recombinant proteins for BMP4, DKK3, ESM1, FN1, IFI30, Ly86, PNRP, SERPINI1, UPP1, and VEGFC separately to the media with cultured c8161 melanoma or HT1080 cells in the plugged plate assays (Figure 4A, B). After the addition of recombinant proteins, rubber stopper plugs were removed and measurements of cell positions revealed that BMP4, ESM1, FN1, IFI30, and VEGFC stimulate cell migration, resulting in a significant increase in the area of open free space covered by the invading c8161 melanoma cells (Figure 4C). The addition of SERPINI1 led to a similar observation in c8161 cells, but the change was only significant in HT1080 fibrosarcoma cells (Figure 4C). High c8161 melanoma cell density in culture was also observed after the addition of exogenous protein for UPP1, without increased cell migration (data not shown). A decrease in uniform density with increased clustering was observed in c8161 melanoma cells after the addition of DKK3 (Figure 4B, C).

2.7 | Knockdown of BMP4 by siRNA inhibits in vivo c8161 melanoma cell invasion in a chick embryo transplant model, but invasion may be rescued in vitro after addition of BMP4 recombinant protein

We first performed a Go Term analysis of genes up-nd down-regulated in BMP4siRNA compared to WT control (Figure 5A, B). Go Term analysis of the 152 genes down-regulated in BMP4siRNA treated c8161 cells increased emphasis on cell migration, growth, and differentiation (Figure 5B). We next performed a Go Term analysis of genes up-nd down-regulated on recombinant BMP4 treated cells compared to WT control (Figure 5C, D). Go Term analysis of the 248 genes up-regulated after treatment with BMP4 increased emphasis on cell migration and motility (Figure 5D).

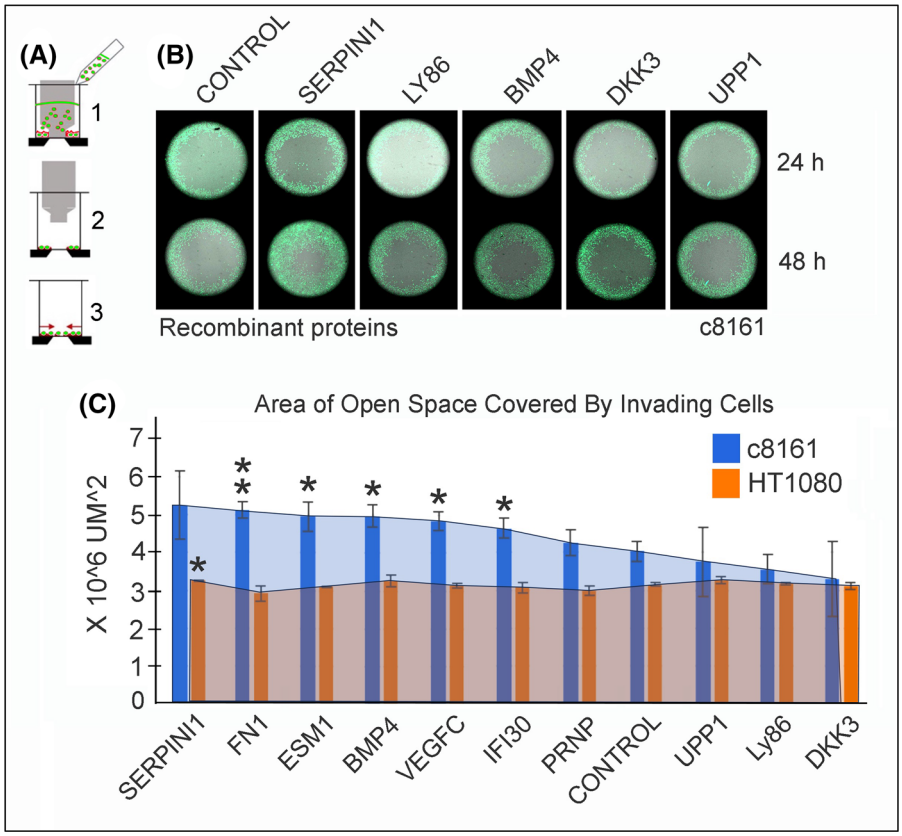

FIGURE 4 Recombinant proteins affect migration of human c8161 melanoma cells into open free space in culture. (A) c8161 cells were seeded into plugged 96-well plates and plugs were removed after 24 h; recombinant proteins were added to the culture media. Cell plates were imaged at +24 h and at 48 h after plug removal, and cell positions were recorded and scored. (B) Typical examples of c8161 melanoma cell positions at 24 h (top row) and 48 h (bottom row) after plug removal and addition of recombinant protein. (C) Compared to control (PBS), c8161 cells in the presence of VEGFC ($p = .0186$), BMP4 ($p = .0134$), ESM1 ($p = .0262$), IFI30 ($p = .0469$), and FN1 ($p = .0049$) significantly increased migration into the open free spaces. SERPINI1 was the only recombinant protein to affect migration of HT1080 cells ($p = .0451$). All recombinant proteins were used at 50 ng/mL added to the culture media. c8161 cells (blue bars) and HT1080 cells (orange bars) with p-values calculated as * = $p < .05$, ** = $p < .01$.

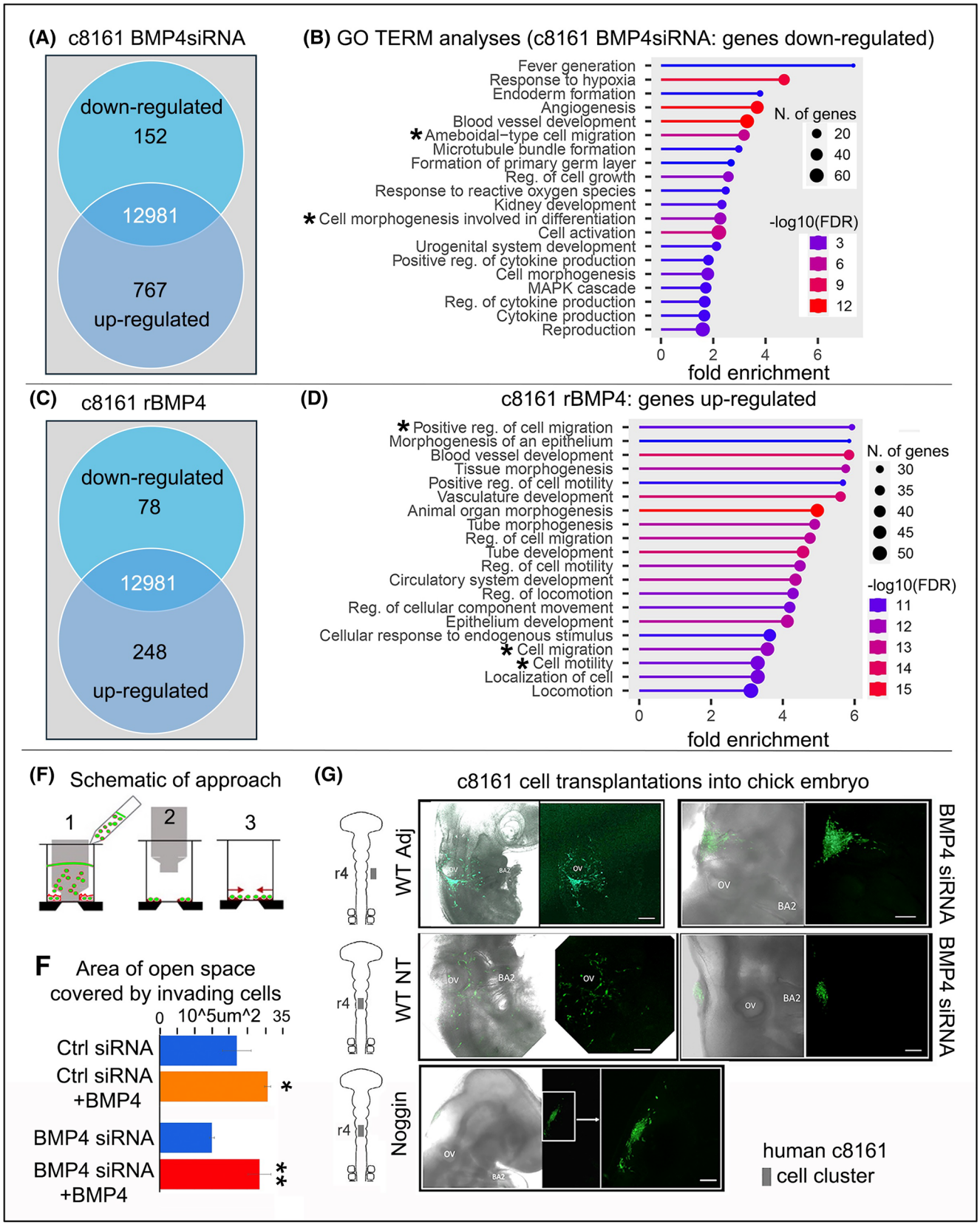

FIGURE 5 Legend on next page.

The discovery that several recombinant proteins of the 45-gene panel stimulate c8161 melanoma cell invasion and migration suggested potential synergy experiments to rescue invasive cell behaviors after gene knockdown. To test this, we knocked down the function of BMP4 by siRNA in c8161 cells, then loaded cells into the rubber stopper assay (Figure 5E). After 24 h, BMP recombinant protein or control (PBS) was added to the culture media, and the rubber stopper barrier was removed (Figure 5E). Measurements of the area covered by c8161 melanoma cells showed a significant decrease after only BMP4 siRNA knockdown (PBS control, Figure 5F). However, the addition of BMP4 to the culture media stimulated c8161 melanoma cell migration so that nearly double the area was covered by invasive cells, even with BMP4 siRNA targeted to the cells (Figure 5F). To test whether knockdown of BMP4 inhibits in vivo cell invasion and migration, we transplanted c8161 human melanoma cells treated with BMP4 siRNA knockdown into our chick embryo transplant model. Briefly, cells were grown in a hanging drop and transplanted into the chick hindbrain (at the level of approximately r4) or adjacent to r4 (Figure 5G) and allowed to invade with host NC cells for 48 h (described in[14]). We measured the maximum diagonal of the bounding box surrounding the GFP-positive graft. WT controls migrated 186 μm (adjacent graft) and 107 μm (neural-tube graft), whereas BMP4-siRNA cells reached only 103 and 43 μm, respectively. Because these values derive from a single embryo per condition, inferential statistics cannot be applied, as an estimate of within-group variance is required to calculate a *p*-value. We therefore present the numbers descriptively. Together, we find that BMP4 siRNA treated c8161 melanoma cells transplanted into the chick neural tube became considerably less invasive (Figure 5G), with slightly lesser effects when transplanted adjacent to the hindbrain (Figure 5G). Treatment of the c8161 melanoma cells with Noggin (a BMP4 antagonist) showed a reduction in cell invasion and migration from the chick neural tube (Figure 5G).

3 | DISCUSSION

Previous single-cell profiling of chick cranial NC cell migratory streams provided a basis to compare a novel transcriptional signature of the migratory stream wavefront with gene signatures obtained from a broad range of other cell invasion phenomena.[11] This produced a 45-gene panel too time-consuming and impractical for single gene in vivo functional studies in an embryo model system, but appropriate for an siRNA high-throughput screening assay. Comparison of changes in cell behaviors and cell number after each of 45 siRNA gene knockdowns in NC-derived human c8161 metastatic melanoma cells versus non-NC-derived HT1080 fibrosarcoma cells converged on a subset of 14 out of 45 genes that significantly impacted cell invasion. Confocal time-lapse imaging of each well of the rubber stopper high-throughput screening assay provided a very large set of cell trajectory data invading into open free space, sufficient for statistical analysis and application of a novel deep learning attention network analysis of cell neighbor relationships of both leading (edge) and follower (bulk) subpopulations. Statistical analysis of in vitro cell behaviors identified 14 out of 45 genes critical to cell invasion and migration, which we ranked as the top six out of 14 (BMP4, ITGB1, IFI30, KCNE3, PRKCQ, and RASGRP1). Deeper analysis of leader versus bulk cell motility data revealed four out of the six genes significantly impaired leader cell motility (BMP4, ITGB1, KCNE3, and RASGRP1). Deep learning then identified two out of the four genes that dramatically altered cell attention patterns (BMP4 and RASGRP1) and unexpected changes in cell-neighbor communication in four out of the 45-gene panel (DAB2, CA2, FN1, and CTNNB1). The statistical and deep learning analyses further validated the other eight out of the 14 genes as previously implicated in other cell migration and invasion studies (FN1, FOS, IL13RA1, KYNU, NEXN, SH3TC1, UPP1, and VIM). Functional experiments testing 10 out of the 11 known secreted molecules of the 45-gene panel

FIGURE 5 Gene expression analysis of BMP4 mis-expression in metastatic melanoma c8161 cells reveals regulation of cell migration genes and changes in cell migration after transplant into the chick embryo transplant model. (A) Genes up-and down-regulated in BMP4siRNA compared to WT control. (B) Go Term analysis of the 152 genes down-regulated in BMP4siRNA treated c8161 cells, increased emphasis on cell migration, growth and differentiation. (C) Genes up-and down-regulated on recombinant (r) BMP4 treated cells compared to WT control. (D) Go Term analysis of the 248 genes up-regulated after treatment with BMP4, increased emphasis on cell migration and motility. (E)–(G) Exogenous BMP4 rescues BMP4 siRNA knockdown in human c8161 melanoma cells in culture. (E) Schematic of the plugged plate approach: (1) c8161 cells were seeded into plugged 96-well plates after BMP4 siRNA knockdown; (2) plugs were removed after 24 h. BMP4 recombinant protein was then added to the culture media at 50 ng/mL; (3) Cell plates were imaged at +24 h after plug removal and cell positions were recorded and scored. (F) The area covered by invading c8161 melanoma cells was measured and compared for four scenarios including control siRNA, control siRNA+BMP4, BMP4 siRNA, and BMP4 siRNA+ BMP4. (G) Typical examples of human c8161 melanoma cell positions after knockdown of BMP4 by siRNA or Noggin treatment and transplantation into the chick hindbrain (~r4 level) or the adjacent paraxial mesoderm and 3D-confocal images collected at +24 h. *p*-values calculated as * = $p < .05$, ** = $p < .01$.

showed five out of 10 stimulated cell migration when added to the culture media (BMP4, ESM1, FN1, IFI30, and VEGFC); knockdown of BMP4 and subsequent transplantation of c8161 cells into an in vivo embryo model reduced invasion. Together, these results distilled the 45-gene panel into a tractable subset of genes for further studies of collective cell migration and invasion.

The top six out of the 14 genes we identified from the 45-gene panel whose knockdown significantly affected free space closure did so with changes in c8161 melanoma cell motility rather than cell proliferation. Key to accurately making this distinction was the use of a rubber stopper in the high-throughput assay, which overcame the problems of rupturing cell membranes at the wound edge and creating a non-uniform invasive wavefront, typical of scratch assays. This allowed for a more accurate means to collect fluorescently labeled cell trajectory data of an invasive migratory wavefront and distinguish leading edge versus bulk follower cell movements. While gene knockdown was not utilized to assess whether the other 31 out of the 45 gene panel that did not show a phenotype was due to lack of siRNA function, we did utilize three different siRNAs to target different regions of each of the 45 genes. Using this as an initial screening approach allowed us to rank the targets by level of interest for further experiments.

Deep learning attention network analysis identified two key aspects of cell–cell neighbor interactions from the high-throughput assay cell trajectory data. First, there were clear differences in collective attention between the c8161 melanoma versus HT1080 fibrosarcoma cells—the latter was used as a negative non-NC derived cell line control (Figure 3). For the HT1080 cells, the network analysis determined that the most influential neighbors were the leader directly in front of and the follower directly behind the focal cell (Figure 3). This was somewhat expected given the known cell behavior of HT1080 cells moving in strongly aligned chains of cells in a leader-follower manner.

In contrast, the collective attention network for c8161 melanoma cells determined the most influential neighbors to be within a wide front ahead of and to the sides of the focal cell (Figure 3). This analysis is consistent with observations of the collective migratory behaviors of the c8161 melanoma cells, edge versus bulk subpopulations (Figure 3). Second, in several cases in which one of the 45 gene panels was knocked down, there was a wide range of striking changes to the c8161 melanoma cell wildtype attention map, including an expansion of the cell–cell neighbor interactions along the sides and to the rear of the focal cell, and even a switch to the follow the leader directly in front pattern (Figure 3). When we asked whether altered patterns of attention were associated with the observed free space closure changes for the top four gene knockdowns leading to significantly reduced free space closure (BMP4, ITGB1, KCN3, and RASGRP1), we learned that only BMP4 and RASGRP1 knockdowns displayed altered attention patterns (Figure 3E). Loss of BMP4 displayed a reduced forward attention map and a long-range connection with cells in the rearward direction, including a curious gap directly behind the focal cell (Figure 3). Observations of dynamic cell behaviors after lossoffunction of BMP4 clearly showed how loss of directionality of leader cells created gaps with follower cells (stream separation) to disrupt collective cell migration (Figure 2I; Movie 1), helping to explain why the cell attention map was altered (Figure 3E). In contrast, loss of RASGRP1 showed an expanded attention map to the front and sides of the focal cell (Figure 3). Time-lapse observations after RASGRP1 lossoffunction were consistent with the changes in the cell attention map, as leader cells were less directional and escaped contact with followers (Figure 2I; Movie 1). Loss of ITGB1 and KCNE3 retained the wildtype c8161 melanoma cell attention map (Figure 3D).

We unexpectedly learned of major alterations to the cell attention maps after loss-of-function of DAB2, CA2, FN1, and CTNNB1; genes that did not correlate with a significant reduction in free space closure except for FN1 (Figure 3D, F). For example, after loss of DAB2, cells appeared to expand communication with neighbors along the sides of a cell rather than simply directly in front of the cell in search of open free space. DAB2, which encodes a mitogen-responsive phosphoprotein, has been shown to regulate the in vitro migration and invasion of prostate cancer cells.[18] Its knockdown by shRNA inhibits these characteristics in PC3 cells in vitro, but the mechanism of its action remains unclear. In our hands, when DAB2 was knocked down by siRNA, c8161 melanoma cells altered their cell neighbor relationships to include a much wider attention field (Figure 3D), suggesting cells lost a sense of individual directed movement; however, overall we did not observe a significant reduction in free space closure in vitro. These observations suggest that either DAB2 may not be critical for melanoma migration or, alternatively, knockdown causes cells to seek alternative guidance signals.

This study is the first to use attention maps in the context of a high-throughput experiment, and for this reason, it has found novel spatial patterns of cell–cell communication not previously discovered in other studies. Extensive future work is needed to correlate these computational findings with the mechanistic causes of why cell–cell interactions seem to be spatially altered. This will involve both experiments of high complexity and mathematical modeling. For example, combining

fluorescently labeled cell membranes and nuclei to track cell positions and measure cell–cell contacts would help to interpret the findings of our deep learning approach presented here by linking changes in cell neighbor influence with perhaps disruption of cell–cell contacts. We also recognize the need to expand the number of cell lines analyzed, having focused here on human c8161 metastatic melanoma. This would help to provide further supporting evidence for a critical role in cell migration and invasion of the small subset of genes we identified. For example, whether these genes also play a similar role in NC-derived neuroblastoma would be interesting to pursue and represent a broader context. We recognize that the experiments to test whether knockdown of the critical subset of genes discovered in vitro have a role in in vivo cell invasion and migration only considered BMP4 (Figure 5G). Although these results were encouraging, future in-depth studies are needed and expanded to the other genes within the critical subset to more fully substantiate our results. Finally, a limitation of the present screen is the absence of gene-by-gene knock-down quantification, so some non-hits may reflect subthreshold silencing; future work will pair qPCR or western validation with targeted rescue experiments to resolve such cases.

The addition of recombinant proteins into the culture media to rescue migration of siRNA-treated c8161 melanoma cells further supported a role for BMP4 and identified potential future gene synergy experiments. The addition of recombinant proteins into the culture media of c8161 melanoma and HT1080 fibrosarcoma cells for 10 out of the 11 known secreted molecules of the 45-gene panel (Figure 4A, B) identified five out of 10 molecules (BMP4, ESM1, FN1, IFI30, and VEGFC) that stimulated c8161 cell migration and significantly increased invasion of the open free space area (Figure 4C). Either BMP4 knockdown by siRNA or Noggin strikingly reduced in vivo invasion and migration after transplantation into the chick embryo hindbrain (Figure 5B, C). However, the addition of BMP recombinant protein into the culture media, 24 h after siRNA knockdown, stimulated migration and increased the covered free space area (Figure 4C). SERPINI1 showed a significant change in open free space area with HT10180 cells but was not significant in c8161 cells (Figure 4C). Interestingly, three out of the five secreted molecules that stimulated in vitro c8161 migration were included in the 14 out of the 45-gene panel that reduced c8161 migration after gene knockdown (BMP4, FN1, and IFI30), suggesting potential synergies of reduced versus stimulated migration.

The combination of statistical analysis and deep learning, and subsequent experiments using recombinant proteins and an in vivo chick embryo transplant model supported the critical nature of BMP4 and RASGRP1 in collective cell migration and invasion and stimulate future experiments in collective NC cell migration. RASGRP1 (a Ras guanine nucleotide-releasing factor that activates Ras and its downstream ERK and AKT signaling pathways) has been shown to promote the formation of spontaneous skin tumors and enhance malignant progression in a multi-stage carcinogenesis skin model that relies on oncogenic activation of H-Ras.[19] Similarly, there is previous evidence to support a predominant role for BMP4 in melanoma metastasis, in part through regulation of SNAI2.[20,21] More recent studies have shown that BMP4 enhances the epithelial-to-mesenchymal transition (EMT) and cancer stem cell properties of breast cancer cells via Notch signaling[22] and in gastric cancer cells.[23] Knockdown of BMP4 in gastric cancer cell lines shows reduced migration in vitro scratch assays and reduced tumor growth and spread when injected into the mouse tail vein.[23] When BMP4 siRNA-treated gastric cancer cells are subcutaneously transplanted into the mouse skin, cells show upregulation of E-cadherin and downregulation of Vimentin,[23] all supporting a critical role for BMP4 in cell invasion and migration and further study of downstream targets.

In regards to melanoma, BMP inhibitors show promise at reducing melanoma growth in mouse melanoma models.[24] Together, this encouraged our further examination of BMP4 in NC cell migration. In support of this, we previously observed high induction of BMP4 in c8161 melanoma cells at the migratory wavefront after cell transplantation into the chick embryonic microenvironment.[14] This supported our knockdown of BMP4 in melanoma cells and their reduced migration and invasion after transplantation into the chick embryo NC microenvironment (Figure 5). Thus, further analysis of NC cell behaviors in vitro and in vivo in the chick embryo transplant model after loss of BMP4, RASGFP1, and the other four genes may provide insights into their functional roles in cranial NC cell migration.

The combined statistical and deep learning attention network analyses validated genes previously implicated in cell migration and invasion, including FN1, FOS, IL13RA1, KYNU, NEXN, SH3TC1, UPP1, and VIM. Several of these genes are known to function through cell-ECM interactions to promote invasion and migration. For example, uridine phosphorylase 1 (UPP1) has been implicated in tumor invasion and migration, particularly in lung adenocarcinoma,[25] by influencing the production and degradation of the ECM. UPP1 may also induce the EMT, where cells gain migratory and invasive capabilities. Similarly, fibronectin1 (FN1) promotes in vitro cell invasion and

migration through integrin signaling in human colorectal cancer cell lines and has been shown to be elevated in human colorectal cancer tissue samples.[26] FN1 is highly expressed in cranial NC cells at the migratory wavefront of streams and is thought to play a critical role in cell communication between leaders and followers to promote long-range stream migration.[27] Also highly expressed in the tumor invasive front in clinical tissue samples in a similar manner to chick cranial NC cells,[11] in this case of oral squamous cell carcinoma (OSCC), c-Fos encodes the transcription factor FOS. C-Fos has been implicated in promoting cell invasion in OSCC via the CD44 pathway in HN6 and SCC9 cell lines.[28] Lastly, VIM (vimentin), an intermediate filament protein that forms part of the cell cytoskeleton, has recently been shown to promote metastasis in a mouse model of non-small cell lung cancer.[29] VIM is highly expressed in the chick cranial NC cell migratory wavefront,[11] but its function in collective NC cell migration remains unexplored.

In summary, our study demonstrated the rapid and systematic analysis of a 45-gene panel to converge on a critical subset of genes using a combined experimental, statistical, and deep learning approach. As advances in spatial transcriptomics and single-cell profiling bring us closer to identifying gene sets associated with distinct, dynamic biological processes, so too will upgrades in deep learning and AI algorithms that shorten the time between high-throughput screening and single-gene functional analysis. Deep learning network analysis provided novel insights, but it is an open question how to interpret these attention maps to provide mechanistic insights. In the chick cranial NC model system, it will be interesting to now determine whether the function of the identified critical subset of cell invasion genes is conserved for other NC cell migratory streams throughout the head, heart, and trunk axial levels, and in other vertebrate model organisms. Further understanding of the function of NC cell invasion genes will have direct applications to emerging cell replacement therapies to repair neurocristopathies by providing a molecular blueprint to control transplanted cell behaviors and suggest therapeutic applications to inhibit NC cell-derived cancer metastasis.

4 | EXPERIMENTAL PROCEDURES

c8161 human malignant aggressive melanoma cells were provided by Dr. Mary Hendrix (Children's Memorial Research Center, Chicago, IL) and were maintained in RPMI media supplemented with 10% FBS. HT1080 cells were obtained from ATCC (catalog #CCL-121) and maintained in EMEM media supplemented with 10% FBS. Cells were plated in Oris collagen-coated 96-well plugged assay plates (Platypus Technologies, #CMACC5.101). HT1080 cells were seeded at 35,000 cells/well and c8161 cells at 45,000 cells/well. For siRNA knockdown, three siRNAs targeting each were purchased from Ambion (Silencer Select, standard purification). Cell lines were transfected with siRNAs using xTremeGene siRNA transfection reagent (1ul/well, Roche, #4476093001; standard protocol). Each Silencer Select guide is pre-validated by the manufacturer for ≥70% mRNA depletion in a standard HeLa assay and is optimized bio-informatically to minimize off-target effects. In this high-throughput screen, we did not re-quantify knockdown efficiency for every guide; instead, we defined 'hits' strictly by reproducible phenotypic changes in migration metrics across at least two independent siRNAs. Precise percentage knockdown (mRNA and/or protein) can be determined in subsequent mechanistic studies of the priority genes identified here.

After addition of siRNA transfection mix, 96-well plugged plates were incubated for 48 h (37C, 5% CO_2). Plugs were then removed with the provided plug removal tool (Oris) and 100 μL of fresh media was added to each well. Plates (with lid on) were placed in the Opera Phenix High-Content Screening System (Perkin Elmer; prewarmed to 37°C and 5% CO_2). Images were collected every 30 min for 24 h and processed using NIH Image J.

4.1 | Quantitative analysis

Cell count and wound areas: For the computation of wound areas, we used Fiji to threshold and binarize the nuclear channel to obtain the individual cell locations, and then performed convolution with a Gaussian kernel with a standard deviation of two cell widths to smooth the nuclear channel into a density field. We then thresholded and binarized to obtain wound masks to measure the area of the wound. We used the inbuilt Laplacian of Gaussian (LoG) detector in Fiji to detect spots from the nuclear channel to count cells using Fiji and obtain cell count fold changes between the start and the end of the experiment.

Statistical analysis of fold changes: We computed the area and cell count fold changes for each of the tissues recorded and grouped them together by knockdown, giving sets of 3–9 biological samples for each individual knockdown. We computed z-scores for each of the wound area and cell count fold changes and performed a standard Welch's t-test to compute the

TABLE 2 Computed validation accuracies of the statistical method.

Gene name	
ADM	0.6209
ANXA1	0.6411
ARPC3	0.6383
ATP1B1	0.6190
BMP4	0.6544
CA2	0.6190
COL4A4	0.6201
CREB3L2	0.6228
CTNNB1	0.6179
DAB2	0.6215
DKK3	0.6368
DPYD	0.6183
ESM1	0.6190
FLT1	0.6234
FN1	0.6141
FOS	0.6217
HSPB1	0.6205
HSPB8	0.6388
IFI30	0.6408
IGFBP2	0.6201
IL13RA1	0.5893
INHBA	0.6221
ITGB1	0.6197
JUN	0.6232
KCNE3	0.6194
KITLG	0.6188
KYNU	0.6198
LY86	0.6422
MMP11	0.6188
NEXN	0.6249
NRP1	0.6208
Neg	0.6026
PRKCQ	0.6354
PRNP	0.6380
RAC2	0.6398
RASGRP1	0.6240
RASGRP3	0.6404
SERPINI1	0.6270
SH3TC1	0.6168
TUBB6	0.6105
UNC5B	0.6118
UPP1	0.6015
VEGFC	0.6363
VIM	0.6088
Water	0.6330

corresponding p-values for wound area and cell count fold change.

$$z_j = \sum_{i=1}^{n} \Pi(\alpha_j, a_j) \frac{W(x_j, v_j, v_i)}{\sum_{\ell=1}^{n} W(x_j, v_j, v_\ell)},$$

Table 2 includes validation accuracies.

Individual cell trajectories: We use TrackMate in Fiji to obtain individual cell tracks from the binarized and thresholded images. We use the inbuilt LoG detector with standard LAP tracker in Fiji/TrackMate with no track splitting and merging, as well as a gap closure of five frames and a maximum linking distance of 100 μm. We set the cell diameter for c8161 cells to 20 μm and that for ht1080 cells to 30 μm. From the TrackMate outputs, we filtered for cell tracks that contain at least five consecutive frames.

Classification of edge and bulk cells: We classified cells as edge cells if their distance to the masked wound edge was less than five cell radii at their first detected time point.

Training of deep attention networks: Mathematically, deep attention networks take a collection of individual cell trajectories and seek to forecast the logit probability, z, that a given cell—which we call the *focal* cell—will turn right, given the attributes of its neighbors. In the deep attention framework this is done by learning a pairwise function, Π, that quantifies the influence that the focal cell's neighbors have, as a function of their velocity, distance, and acceleration. At the same time, the deep attention framework learns an *attention function*, W, that places weights according to the apparent attention that cells pay their neighbors.[30,31] Put together, the logit probability that focal cell j will turn right, z_j, is expressed as a function of the interaction between cell j and its neighbors, and weighted according to their relative velocities, where x_j, v_j denote the position and velocity of cell j (cell i, respectively), and α_i is a vector containing the velocity, distance to the focal cell and acceleration of a given cell i. The sum ranges over all neighboring cells i of the focal cell j, and therefore the resulting logit probability is a weighted sum of pairwise interactions between the focal cell and its neighbors. The network receives, for each focal cell, the positions of neighbors whose centers fall between an inner exclusion

radius $r = 15\,\mu m$ and an outer interaction radius $R = 90\,\mu m$ (illustrated by the red circles in Figure 3). Bright yellow pixels in the resulting attention maps correspond to a normalized weight of 1, indicating that neighbors in that angular/radial bin are predicted to exert the strongest influence on the focal cell's next turn; dark-blue pixels correspond to weights close to 0. Importantly, the emergence of a high-weight sector on only one side of the map reveals directional polarity in neighbor influence—one of the central findings highlighted in the "Results" section.

We emphasize that the attention function, W, when normalized, acts like a kernel that assigns different weights to the neighbor cells, depending on their location relative to the velocity of the focal cell. Therefore, if W is not uniform for all spatial locations around the focal cell, the deep attention network framework suggests that the focal cells pay attention to only a subset of their neighbors, rather than all neighbors within a certain distance, making interactions *anisotropic*.

Training of the attention networks is performed as follows. The network architecture for all neural networks is identical across different siRNAs and is chosen to be equal to that employed by Lachance et al.,[30] which is given by three hidden layers of 128 neurons each with ReLU activation after each layer, plus a readout layer of 128 for both the pairwise interaction network and the attention network. We use an Adam optimizer with the same learning schedule as that of LaChance et al.[30] and Polavieja et al. (2019) We set a maximum number of epochs equal to 50,000 training steps and training was stopped if the validation loss did not reach a new minimum for 10 epochs and did increase 25% from the current minimum. In the attention network, the learning rate was annealed from 10^{-4} to 10^{-5}, using a batch size of 500, while in the interaction network, the learning rate was annealed from 5×10^{-5} to 10^{-5}, which were optimal settings previously found by Polavieja et al. (2019) for this framework.

For each siRNA, cell trajectories from all of the corresponding knockdowns are used for training, with trajectories randomly split into a training, validation, and test set. We assess the accuracy of the framework in estimating turning probabilities by analyzing the accuracy of predicting a right turn for each trajectory in the data set for each knockdown. We found that for all siRNAs, this prediction accuracy exceeded 60%.

Training was done with the same hyperparameters as Lachance et al.[30] Training was performed on the Oxford Advanced Research Computing cluster using five 48-core Cascade Lake (Intel Xeon Platinum 8268 CPU @ 2.90GHz) nodes.

ACKNOWLEDGMENTS

PMK would like to thank the generous funding of NIH/NICHD (R03-HD105079-02) for partial support of this study. JCK would like to thank the support of the Stowers Institute core facilities and staff scientists, especially Dr. Jay Unruh. REB is supported by a grant from the Simons Foundation (MP-SIP-00001828).

DATA AVAILABILITY STATEMENT

Trained networks and their inputs will be made available upon reasonable request.

ORCID

S. Martina Perez https://orcid.org/0000-0001-8596-8595
P. M. Kulesa https://orcid.org/0000-0001-6354-9904

REFERENCES

1. Giniunaite R, McLennan R, McKinney MC, Baker RE, Kulesa PM, Maini PK. An interdisciplinary approach to investigate collective cell migration in neural crest. *Dev Dyn*. 2020; 249(3):270-280. doi:10.1002/dvdy.124
2. Szabo A, Melchionda M, Nastasi G, et al. In vivo confinements promote collective migration of neural crest cells. *J Cell Biol*. 2016;213(5):543-555. doi:10.1083/jcb.201602083
3. Szabo A, Theveneau E, Turan M, Mayor R. Neural crest streaming as an emergent property of tissue interactions during morphogenesis. *PLoS Comput Biol*. 2019;15:e1007002. doi:10.1371/journal.pcbi.1007002
4. Friedl P, Hegefeldt Y, Tusch M. Collective cell migration in morphogenesis and cancer. *Int J Dev Biol*. 2004;48(5–6):441-449. doi:10.1387/ijdb.041821pf
5. Friedl P, Alexander S. Cell invasion and the microenvironment: plasticity and reciprocity. *Cell*. 2011;147(5):992-1009. doi:10.1016/j.cell.2011.11.016
6. Kulesa PM, Kasemeier-Kulesa JC, Teddy JM, et al. Reprogramming metastatic melanoma cells to assume a neural crest cell-like phenotype in an embryonic microenvironment. *Proc Natl Acad Sci USA*. 2006;103:3752-3757. doi:10.1073/pnas.0506977103
7. LeDouarin NM, Kalcheim C. *The Neural Crest*. 2nd ed. Cambridge University Press; 1999. doi:10.1017/CBO9780511897948
8. Fitriasari S, Trainor PA. Gene-environment interactions in the pathogenesis of common craniofacial anomalies. *Curr Top Dev Biol*. 2023;152:139-168. doi:10.1016/bs.ctdb.2022.10.005
9. Vega-Lopez GA, Cerrizuela S, Tribulo C, Aybar MJ. Neurocristopathies: new insights 150 years after the neural crest discovery. *Dev Biol*. 2018;444(Suppl 1):S110-S143. doi:10.1016/j.ydbio.2018.05.013
10. Morrison JA, McLennan R, Wolfe LA, et al. Single-cell transcriptome analysis of avian neural crest migration reveals signatures of invasion and molecular transitions. *Elife*. 2017;6: e28415. doi:10.7554/eLife.28415
11. Morrison JA, McLennan R, Teddy JM, et al. Single-cell reconstruction with spatial context of migrating neural crest cells and their microenvironments during vertebrate head and neck formation. *Development*. 2021;148(22):dev199468. doi:10.1242/dev.199468
12. Tatarakis D, Cang Z, Wu X, et al. Single-cell transcriptomic analysis of zebrafish cranial neural crest reveals spatiotemporal

regulation of lienage decisions during development. *Cell Rep*. 2021;37(12):110140. doi:10.1016/j.celrep.2021.110140
13. Stavely R, Hotta R, Guyer RA, et al. A distinct transcriptome characterizes neural crest-derived cells at the migratory wavefront during enteric nervous system development. *Development*. 2023;150(5):dev201090. doi:10.1242/dev.201090
14. Bailey CM, Morrison JA, Kulesa PM. Melanoma revives an embryonic migration program to promote plasticity and invasion. *Pigment Cell Melanoma Res*. 2012;25(5):573-583. doi:10.1111/j.1755-148X.2012.01025.x
15. Bailey CM, Kulesa PM. Dynamic interactions between cancer cells and the embryonic microenvironment regulate cell invasion and reveal EphB6 as a metastasis suppressor. *Mol Cancer Res*. 2014;12(9):1303-1313. doi:10.1158/1541-7786.MCR-13-0673
16. Giuggioli L, McKetterick TJ, Holderied M. Delayed response and biosonar perception explain movement coordination in trawling bats. *PLoS Comput Biol*. 2015;11(3):1-21. doi:10.1371/journal.pcbi.1004089
17. Jiang L, Giuggioli L, Perna A, et al. Identifying influential neighbors in animal flocking. *PLoS Comput Biol*. 2017;13(11):e1005822. doi:10.1371/journal.pcbi.1005822
18. Westcott JM, Prechtl AM, Maine EA, et al. An epigenetically distinct breast cancer cell subpopulation promotes collective invasion. *J Clin Invest*. 2015;125(5):1927-1943. doi:10.1172/JCI77767
19. Sharma A, Paricharak DG, Nigam JS, et al. Histopathological study of adnexal tumours-institutional study in South India. *J Skin Cancer*. 2014;1. doi:10.1155/2014/543756
20. Gupta PB, Kuperwasser C, Brunet JP, et al. The melanocyte differentiation program predisposes to metastasis after neoplastic transformation. *Nat Genet*. 2005;37:1047-1054. doi:10.1038/ng1634
21. Rothhammer T, Poser I, Soncin F, Bataille F, Moser M, Bosserhoff AK. Bone morphogenetic proteins are overexpressed in malignant melanoma and promote cell invasion and migration. *Cancer Res*. 2005;65(2):448-456. doi:10.1158/0008-5472.448.65.2
22. Choi S, Yu J, Park A, et al. BMP-4 enhances epithelial mesenchymal transition and cancer stem cell properties of breast cancer cells via notch signaling. *Sci Rep*. 2019;9:11724. doi:10.1038/s41598-019-48190-5
23. Zhou H, Wang W, Liu M, et al. IDO promotes the proliferation and invasion of prostate cancer cells through KYNU. *Genes and Genomics*. 2023;45:367-376. doi:10.1007/s13258-022-01316-y
24. Kalal BS, Modi PK, Upadhya D, Saha P, Prasad TSK, Pai VR. Inhibition of bone morphogenetic proteins signaling suppresses metastasis melanoma: a proteomics approach. *Am J Transl Res*. 2021;13(10):11081-11093.
25. Li Y, Jiang M, Aye L, et al. UPP1 promotes lung adenocarcinoma progression through the induction of an immunosuppressive microenvironment. *Nat Commun*. 2024;14. doi:10.1038/s41467-024-45340-w
26. Cai X, Liu C, Zhang TN, Zhu YW. Down-regulation of FN1 inhibits colorectal carcinogenesis by suppressing proliferation, migration, and invasion. *J Cell Biochem*. 2018;119:4717-4728. doi:10.1002/jcb.26651
27. Martinson WD, McLennan R, Teddy JM, et al. Dynamic fibronectin assembly and remodeling by leader neural crest cells prevents jamming in collective cell migration. *Elife*. 2023;12:e83792. doi:10.7554/eLife.83792
28. Dong C, Ye DX, Zhang WB, Pan HY, Zhang ZY, Zhang L. Overexpression of c-fos promotes cell invasion and migration via CD44 pathway in oral squamous cell carcinoma. *J Oral Pathol Med*. 2015;44:353-360. doi:10.1111/jop.12296
29. Berr AL, Wiese K, dos Santos G, et al. Vimentin is required for tumor progression and metastasis in a mouse model of non-small cell lung cancer. *Oncogene*. 2023;42:2074-2087. doi:10.1038/s41388-023-02703-9
30. Lachance J, Suh K, Clausen J, Cohen DJ. Learning the rules of collective cell migration using deep attention networks. *PLoS Comput Biol*. 2022;18(4):e1009293. doi:10.1371/journal.pcbi.1009293
31. Heras FJH, Romero-Ferrero F, Hinz RC, de Polavieja GG. Deep attention networks reveal the rules of collective motion in zebrafish. *PLoS Comput Biol*. 2019;15(9):e1007354. doi:10.1371/journal.pcbi.1007354

How to cite this article: Kasemeier-Kulesa JC, Martina Perez S, Baker RE, Kulesa PM. Identification of neural crest and melanoma cancer cell invasion and migration genes using high-throughput screening and deep attention networks. *Developmental Dynamics*. 2025;1-18. doi:10.1002/dvdy.70059